

Article

Simulation and Experimental Study on Continuous Wave Fiber Laser Removal of Epoxy Resin Paint Film on the Surface of 6061 Aluminum Alloy

Yahui Li ¹, Jingyi Li ¹, Hang Dong ¹, Wei Zhang ^{1,*} and Guangyong Jin ^{1,2,*}

¹ Jilin Key Laboratory of Solid-State Laser Technology and Application, School of Physical Sciences, Changchun University of Science and Technology, Changchun 130022, China; 2020200007@mails.cust.edu.cn (Y.L.); 2022800023@cust.edu.cn (J.L.); 2018200001@mails.cust.edu.cn (H.D.)

² School of Electrical and Electronic Engineering, Changchun University of Technology, Changchun 130012, China

* Correspondence: 201600034@cust.edu.cn (W.Z.); jgycust@cust.edu.cn (G.J.)

Abstract: Paint removal is an essential process in the industrial field. Laser technology provides an effective method of paint removal to replace traditional mechanical and chemical methods. This paper establishes a continuous wave (CW) laser thermal paint removal model based on heat conduction theory and Arrhenius' law. The paint stripping process of epoxy paint film on the surface of 6061 aluminum alloy via CW laser was studied through simulation and experiment. We found that the carbonization of the paint film during the CW laser paint removal process will inhibit the laser paint removal process. Therefore, the paint removal efficiency of the CW laser is limited. The depth of CW laser paint removal increases linearly with the CW laser power density. However, during the CW laser paint removal process, due to the pyrolysis of the paint film and the reflection of the laser by the substrate, the surface temperature of the material first increases and then decreases. In addition, after laser paint removal, the surface roughness of the material after paint removal is reduced due to the melting of the base material. The model established in this article can provide a theoretical reference for studying the CW laser paint removal process.

Keywords: CW laser removal paint; laser-paint interaction; surface morphology



Citation: Li, Y.; Li, J.; Dong, H.; Zhang, W.; Jin, G. Simulation and Experimental Study on Continuous Wave Fiber Laser Removal of Epoxy Resin Paint Film on the Surface of 6061 Aluminum Alloy. *Photonics* **2024**, *11*, 82. <https://doi.org/10.3390/photonics11010082>

Received: 16 November 2023

Revised: 27 December 2023

Accepted: 31 December 2023

Published: 17 January 2024



Copyright: © 2024 by the authors. Licensee MDPI, Basel, Switzerland. This article is an open access article distributed under the terms and conditions of the Creative Commons Attribution (CC BY) license (<https://creativecommons.org/licenses/by/4.0/>).

1. Introduction

In the industrial field, the surface of large equipment is painted to protect it, to prevent corrosion, and to increase its service life. After the equipment has been used for a while, the paint film on the surface must be removed and repainted after the paint film ages and becomes stripped due to environmental influences. Due to various surface cleaning methods such as traditional chemical, grinding, and sandblasting methods, there are problems such as the scattering of dust containing harmful substances. The quality of the paint film after repainting is closely related to the surface quality of the substrate, and these problems will reduce the repainted paint film's quality. When traditional chemical and mechanical methods are used to remove paint and repaint, the quality of the repainted paint film could be poor [1]. To solve these problems, high-precision, green, and environmentally friendly laser cleaning technology can be used to replace these traditional cleaning techniques. Therefore, laser cleaning technology has attracted more and more attention.

Recently, there have been many research reports on CW laser cleaning. Barletta et al. used a CW semiconductor laser to clean the epoxy resin paint on the surface of an aluminum plate. They found that as the laser power density increased, the influence of scanning speed and defocus on the cleaning depth became smaller [2]. Laser power and action time will significantly affect the paint removal effect. Within the appropriate laser parameter range, non-destructive paint removal on the substrate can be achieved [2].

Schmidt et al. used CW diode lasers to remove epoxy resin and chlorinated rubber on steel and concrete surfaces. They found that the paint removal rate increased linearly with laser power density [3]. Turner et al. used a CW CO₂ laser to clean contaminated titanium alloy aerospace parts and found that the paint removal rate increased linearly with laser power [4]. In addition, Chen et al. compared the performance of CO₂ laser, Nd:YAG laser, and abrasive polishing technology in removing marine paint. It was found that the surface roughness of the material after laser cleaning was higher [5]. Madhukar et al. found that ash residue exists on the surface of the substrate after CW laser cleaning. With the assistance of water jets, laser beams can effectively remove paint and residual ash from the substrate surface [6,7]. Guerrero et al. compared the laser paint removal and thermal paint removal processes and found that the efficiency of laser paint film removal was much lower than that of pyrolysis removal [8]. Anthofer et al. used a 10 kW CW diode laser to remove epoxy resin paint contaminated with polychlorinated biphenyls (PCBs) on the concrete surface. It was found to be more efficient than traditional decontamination techniques. At the same time, optimization of the laser device's airflow system resulted in higher decontamination and degradation rates during paint removal [9,10]. Lu et al. used CW laser cleaning technology to clean paint from the surface of aluminum alloy substrates. By analyzing the surface morphology of the substrate after laser cleaning, it was found that when the laser power density is 11.9 W/cm², the performance of the substrate after laser cleaning has better corrosion resistance and surface roughness [11]. Penide et al. used a CW laser to remove graffiti from a stone surface and found that the CW mode has a better cleaning effect than the modulated wave mode. The threshold for lossless paint removal of graffiti on stone surfaces in CW mode is 800 W/cm² [12]. Provinces et al. used a CW laser to remove coatings from steel surfaces. They found that CW laser ablation coating systems can remove most coatings 2–27 times faster than pulsed laser ablation coating systems [13]. Li et al. used a nanosecond laser to remove paint film from the surface of aluminum alloy. The mechanism is thermal decomposition, evaporation, and stripping [14]. Zhao et al. found that as the laser energy density increases, the thickness of paint removal gradually increases, forming a new surface topography with physical properties such as corrosion resistance, anti-reflection, and hydrophobicity [15]. Liu et al. used a water jet-assisted quasi-continuous laser to clean the epoxy resin coating on the surface of 304 stainless steel. It was found that under low energy density and low spot overlap, the cleaning mechanism is mainly the thermal ablation effect. Due to the high energy density and high spot overlap rate under the conditions, the cleaning mechanism is mainly the combined effect of the thermal ablation and plasma shock effects [16].

From the above research, we found that people have studied CW laser paint removal on the surfaces of different materials. However, current CW laser paint removal research mainly focuses on the experiment, and there are few simulation studies on CW laser paint removal, since the CW laser paint removal effect is closely related to its paint removal mechanism. By combining theory and experiment with quantitative analysis of CW laser's ablation paint removal, in-depth research on the CW laser paint removal mechanism can help improve the CW laser paint removal effect.

This paper establishes a CW laser thermal paint removal model based on heat conduction theory and Arrhenius' law. The novelty of this work lies in considering the vaporization of the paint film/carbon shell and the influence of the interface layer between the paint film and the substrate on the heat transfer process, establishing the theory and simulation model of CW thermal paint removal. The CW laser paint removal was studied through simulation and experiments. We analyzed the experimental and simulation results and found that the established CW laser thermal paint removal model can predict the CW laser paint removal threshold. This method can provide a theoretical reference for studying CW laser paint removal. The CW laser paint removal helps reduce the cost of laser paint removal, thereby realizing the widespread application of laser paint removal technology.

2. Theory Model

During CW laser paint removal, the thermal effect is the strongest due to the longer duration and more considerable total power of the CW laser. Ablation is the primary paint removal mechanism during CW laser paint removal. The temperature of the paint film increases rapidly after CW laser action. As the temperature rises, pyrolysis, gasification, combustion, and other phenomena will occur on the surface of the paint film. Since the main component of the paint film is polymer, residual carbon shells will be generated on the material's surface after the paint film gasification. The thermal conductivity of the carbon shell is very low, and its surface temperature rises rapidly after absorbing laser energy. The carbon shell will gasify and ablate as the temperature increases, revealing a bright substrate. To study the mechanism of CW laser paint removal in-depth, a CW laser thermal ablation paint removal model was established based on the heat conduction equation and Arrhenius law, considering the paint film and carbon shell's gasification.

2.1. CW Laser Ablation Paint Removal Model

During the CW laser paint removal, the carbon shell remains on the paint film surface after the paint film gasification. The paint film and carbon shell must be removed during CW laser paint removal to remove the paint entirely and expose the bright substrate. After the paint film and carbon shell gasification, the gasification plume spreads outward and dissipates rapidly. It is assumed that the area after the paint film is gasified and pyrolyzed, and the carbon shell gasification becomes air to simulate material removal.

The physical process involves changes between three substances: paint film, carbon shell, and air. Since the physical process is relatively complex, so is describing this physical process and tracking the phase change interface. We use Arrhenius's law to calculate and track the gasification phase change process of the paint film and carbon shell.

$$Q_j = -\rho L_j \frac{\partial \theta_j}{\partial t}, \quad (1)$$

$$\frac{\partial \theta_j}{\partial t} = \delta(T)(1 - \theta_j) A_j e^{-\frac{\Delta E_j}{RT}}, \quad (2)$$

$$\rho c = \theta_j \rho_i c_i + (1 - \theta_j) \rho_j c_j, \quad (3)$$

$$k = \theta_j k_i + (1 - \theta_j) k_j, \quad (4)$$

$$\delta(T) = \begin{cases} 1 & T \geq T_v \\ 0 & T < T_v \end{cases}, \quad (5)$$

where $j = 1, 2$ represents the paint film and carbon shell, $i = j + 1 = 2, 3$ represents the thermal parameters of the carbon shell and air, Q_j is the heat loss caused by the gasification of the paint film and the carbon shell, A is the pre-exponential reaction index, θ is the mass fraction of the material, ρ is the density of the material, c is the specific heat capacity of the material, k is the thermal conductivity of the material, ΔE is the reaction activation energy of gasification of the material, L is the gasification latent heat of the material, T_v is the gasification temperature of the paint film.

When the CW laser power density is large, the CW laser will cause the substrate to melt and cause its thermal parameters to change. We use the apparent heat capacity method to describe the melting process of aluminum alloy substrates, specify the properties of phase change materials based on the apparent heat capacity formula, and solve the heat conduction equation.

When the material reaches the melt phase transformation temperature T_n of the aluminum alloy substrate, it is assumed that the transformation occurs in the temperature interval between $T_n - \Delta T/2$ and $T_n + \Delta T/2$. In this interval, the material phase of the aluminum alloy substrate is represented by the smooth function θ_n ($n = 1, 2$), which is equal

to 1 before $T_n - \Delta T/2$ and equals 0 after $T_n + \Delta T/2$. The aluminum alloy material's density, specific heat capacity, and thermal conductivity can be expressed as

$$\rho = \sum_{n=1}^2 \theta_n \rho_n \tag{6}$$

$$c = \frac{1}{\rho} \left(\sum_{n=1}^2 \theta_n \rho_n C_n \right) + H_m \frac{\partial \alpha}{\partial T} \tag{7}$$

$$k = \sum_{n=1}^2 \theta_n k_n \tag{8}$$

$$\sum_{n=1}^2 \theta_n = 1 \tag{9}$$

The indices $n = 1$ and 2 represent aluminum alloy and melted aluminum alloy, respectively, H_m is the latent heat of the fusion of aluminum alloy. The mass fraction α can be expressed as

$$\alpha = \frac{1}{2} \frac{\theta_2 \rho_2 - \theta_1 \rho_1}{\theta_1 \rho_1 + \theta_2 \rho_2} \tag{10}$$

Heat loss from the system occurs due to the gasification of the material. The energy loss caused by gasification and ablation is considered at the interface of material phase change, and the heat conduction equation is modified to ensure energy conservation. The modified heat conduction equation can be expressed as

$$\rho c \frac{\partial T}{\partial t} = \nabla \cdot (k \nabla T) + Q_L(t) + \varepsilon \sigma (T_{ref}^4 - T_{surface}^4) + \delta(T) h_1 |_{z=0} (T_{ext} - T_{ref}) + h_2 (T_{ext} - T_{ref}) \tag{11}$$

where ε is the thermal radiation coefficient, σ is the Stefan–Boltzmann constant, $Q_L(t)$ is the CW laser heat source, $h_1 = 50$ (W/(m²·K)) and $h_2 = 10$ (W/(m²·K)) are the convective heat flux on the laser ablation surface and the natural convection heat flux, respectively. The reference temperature is $T_{ref} = 293.15$ K. The T_{ext} , and $T_{surface}$ are the material's external and surface temperatures, respectively.

Since there is an aluminum oxide film with a thickness of about 10μm on the aluminum alloy's surface, the oxide film's influence on the heat transfer process must be considered. Since the surface of the oxide film is rough, there is a mixture of the paint film and aluminum oxide at the interface between the paint film and the aluminum alloy substrate.

The adsorption interface between the paint film and the aluminum alloy substrate is assumed to be the interface layer. The thermal parameters of the interface layer are the average values of aluminum and the paint film. Since the average height of aluminum alloy surface roughness is 2 μm, the thickness of the interface layer is 2 μm. When considering the influence of the interface layer and the aluminum oxide film during the CW laser paint removal, the boundary conditions can be expressed as

$$-n_d \cdot q_d = -\frac{1}{2} \sum_{j=1}^2 d_{sj} \rho_{sj} C_{sj} \frac{\partial T_d}{\partial t} - \frac{(T_u - T_d)}{R_s} \tag{12}$$

$$-n_u \cdot q_u = -\frac{1}{2} \sum_{j=1}^2 d_{sj} \rho_{sj} C_{sj} \frac{\partial T_u}{\partial t} - \frac{(T_d - T_u)}{R_s} \tag{13}$$

$$R_s = \frac{d_{tot}}{k_{tot}} \tag{14}$$

where R_s is the thermal resistance, and the subscripts u and d represent the interface layer between the paint film and the aluminum oxide film and the upper and lower surfaces of the aluminum oxide film, respectively. The $j = 1$ and 2 represent the interface layer and the aluminum oxide layer. The ρ_{sj} , C_{sj} , k_{sj} , and d_{sj} are the density, specific heat capacity, thermal conductivity, and thickness of layer j , respectively. d_{tot} and k_{tot} , are defined as

$$d_{tot} = \sum_{j=1}^2 d_{sj} \tag{15}$$

$$k_{tot} = \frac{d_{tot}}{\sum_{j=1}^2 \frac{d_{sj}}{k_{sj}}} \tag{16}$$

According to the calculation formula of laser thermal penetration depth $l_T = 2 (kt_1/\rho c)^{1/2}$ and the calculation formula of light penetration depth $l_L = 1/\alpha_1$, where t_1 is the laser action time, α_1 is the laser absorption coefficient of the paint film. When the CW laser action time is 1 s, it can be found that the thermal penetration depth l_T (51 μm) of the CW laser is greater than the light penetration depth l_L (26 μm) [17]. The heat source of a CW laser can be regarded as a body heat source. The laser heat source of the CW laser can be divided into reflection, transmission, and absorption. Considering the material as the coordinate system, the material is in the fourth quadrant of the coordinate axis, and the laser heat source can expressed as [18]

$$Q(t) = \frac{2P}{\pi w^2} \exp\left[-2\left(\frac{r}{w}\right)^2\right] (1 - R)\eta_1(t) \tag{17}$$

$$Q_L = Q_{aL} + Q_{rL} + Q_{tL} \tag{18}$$

$$Q_{aL} = \eta_2(\theta_2)Q(t)(\alpha_1\theta_1 + \alpha_2\theta_2)\exp((y - \Delta h)(\alpha_1\theta_1 + \alpha_2\theta_2)) \quad 0 > y > -d \tag{19}$$

$$Q_{rL} = \eta_2(\theta_2)\eta_3(T)Q(t)\exp(-\alpha_2d)(\alpha_1\theta_1 + \alpha_2\theta_2) \exp(-(y + d - \Delta h)(\alpha_1\theta_1 + \alpha_2\theta_2)) \quad 0 > y > -d \tag{20}$$

$$Q_{tL} = (1 - \eta_3(T))Q(t)\exp(-\alpha_2d)\alpha_3\exp((y + d)\alpha_3) \quad y < -d \tag{21}$$

where w is the spot radius of the CW laser, P is the laser power, and R is the reflectivity of the paint film material to the laser. The Δh is the CW laser ablation depth, d is the paint film thickness, and α_2 and α_3 are the laser absorption coefficients of carbon shell and aluminum alloy, respectively.

The step function η_i can be expressed as

$$\eta(t) = \begin{cases} 0 & \text{else} \\ 1 & 0 < t < t_1 \end{cases} \tag{22}$$

$$\eta_1(\theta_2) = \begin{cases} 1 & \theta_2 < 0.99 \\ 0 & \theta_2 > 0.99 \end{cases} \tag{23}$$

$$\eta_2(T) = \begin{cases} 0.92 & 0 < T < T_m \\ 0.8 & T > T_m \end{cases} \tag{24}$$

where $\eta(t)$ is the time distribution function of the CW laser, $\eta_1(\theta_2)$ represents the absorption rate of the paint film/carbon shell to the laser, $\eta_2(T)$ is the reflectivity of the metal material to the laser, T_m is the melting point of the material.

2.2. CW Laser Paint Film Removal Condition

The CW laser’s paint film removal condition is defined as the ablation depth greater than or equal to the paint film thickness.

$$\Delta h = \int_0^{t_1} \frac{\partial \theta_2}{\partial t} dt \geq d \tag{25}$$

where $\frac{\partial \theta_2}{\partial t}$ is the CW laser ablation speed.

The materials used in this study’s simulation model are epoxy resin (coating) and 6061 aluminum alloy (substrate), and their corresponding mechanical parameters are shown in Table 1.

Table 1. Thermal parameters of the materials used in the simulation.

Properties	Paint	Carbon Shell	Aluminum Alloy [19]	Melting Aluminum Alloy [19]	Alumina [20]	Interface Layer
Specific heat capacity C_p (J/kg·K)	1800 [21]	1048 [22]	1050	921	600	1200
Thermal conductivity k (W/(m·K))	0.2 [23]	0.1	223	106	27	13.55
Density ρ (kg/m ³)	1700 [24]	1005 [22,25]	2549	2224	3600	2650
Pre-exponential reaction constant A (m/s)	3×10^{10} [21]	3×10^5 [26]				
Latent heat of fusion L_m (J/kg)			3.89×10^5			
Reaction activation energy of gasification ΔE (kJ/mol)	70 [27]	149.7 [28]				
Latent heat of gasification L_v (J/kg)	2.051×10^5 [27]	2.62×10^7 [26]		1.05×10^7		
The absorption coefficient of the material α (1/m)	5×10^4 [29]	2.5×10^4				
Emissivity ε (1)	0.79 [21]		0.09			
Melting temperature T_m			933 K			
Gasification temperature T_v (°C)	500	600				

3. Experiment

To conduct CW laser paint removal experiments, we built a CW laser paint removal system. The schematic diagram of the experiment is shown in Figure 1. The 6061 aluminum alloy and paint film thicknesses are 1 mm and 0.026 mm, respectively, and the size is 40 mm × 40 mm. It includes a 1070 nm CW laser, focusing lens, photodetector, and high-speed infrared thermometer (IMGA740). The 1070 nm CW laser (IPG YLR-14) is used to

remove the paint film on the surface of the aluminum alloy. Through the photodetector and oscilloscope, we determine that the CW laser time waveform is a square wave lasting 1 s. The spot of the CW laser is a Gaussian beam, the maximum power is 500 W, and the beam quality is less than 1.1. The laser spot is focused to a diameter of 1.5 mm through the ($f = 100$ mm) focusing lens. After the photodetector detects the laser-scattered light, it triggers the DG645 pulse delay generator through the rising edge signal. The DG645 pulse delay generator triggers the rapid thermometer to measure changes in material surface temperature. After the laser paint removal, the material's surface morphology and 3D surface profile are measured using a metallographic microscope and a three-dimensional surface measuring instrument.

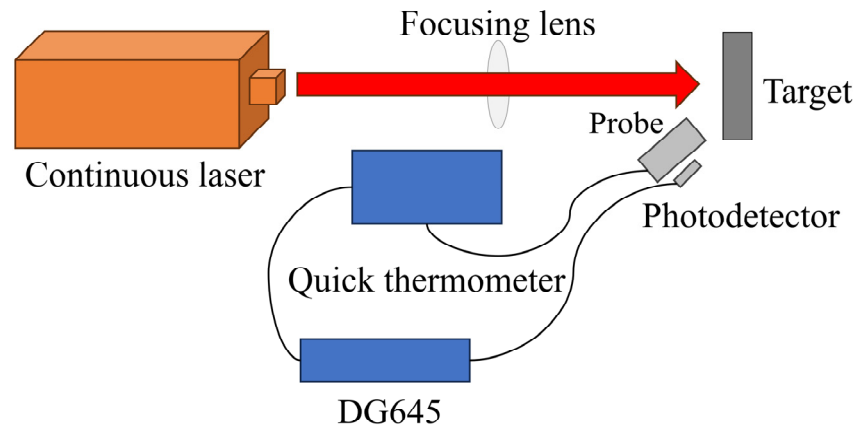


Figure 1. Schematic diagram of the CW laser paint removal experiment.

4. Numerical Model

Figure 2 is a flowchart of the simulation steps. According to the process in Figure 2, the finite element model of thermal coupling is established through COMSOL 6.0 finite element software. By solving this finite element model, we obtain the temperature and ablation depth of the material during CW laser paint removal.

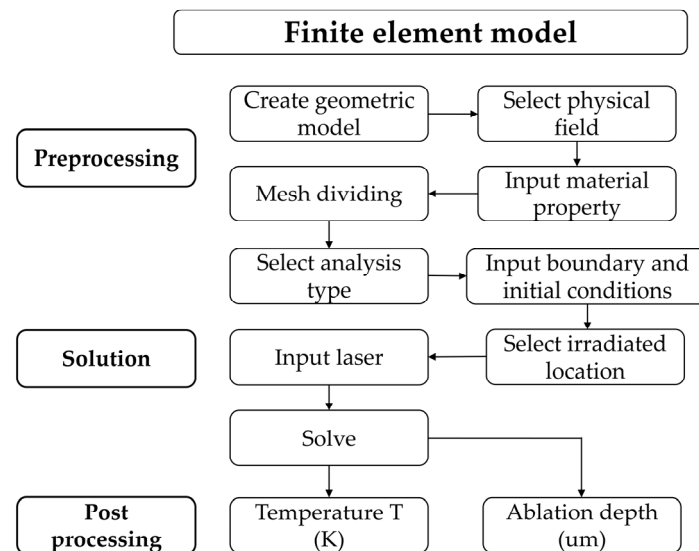


Figure 2. Flowchart of simulation steps.

A continuous wave (CW) laser thermal paint removal model is established using COMSOL 6.0 finite element modeling (FEM) software. Figure 3 shows the model's mesh details. The coordinate system is two-dimensional, and the x-axis and y-axis are the coordinate axes. The aluminum alloy substrate and paint film thickness are set to 1 mm and

0.026 mm, respectively. We use free triangle meshes to mesh the aluminum alloy substrate and paint film, and the meshes are ultra-fine meshes and ultra-fine meshes, respectively. The full mesh contains 205,861 domain elements and 4692 boundary elements. Since the laser spot diameter is 1.5 mm, the length of the material is set to 4 mm. To simulate the paint removal process, the left and right sides are set as infinite element domains and stretched 18 mm to the left and right.

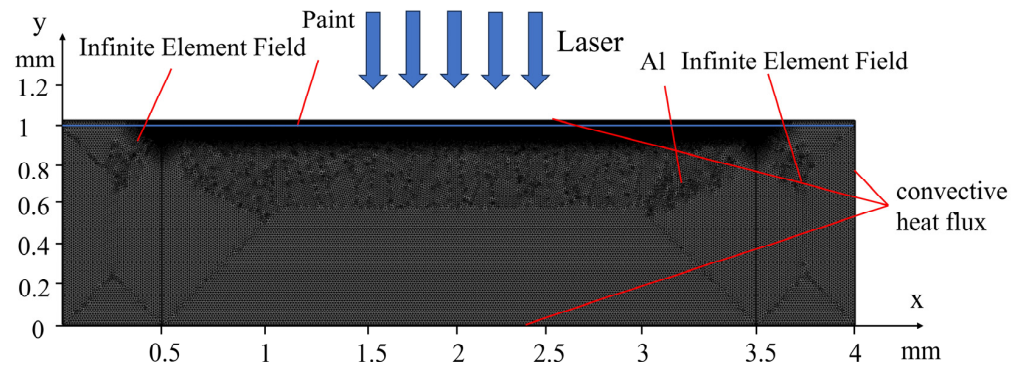


Figure 3. Mesh division of 2D finite element model.

5. Results and Discussion

5.1. Surface Morphology

Figure 4 shows the simulation calculation results of CW laser paint ablation. It can be found that as the laser power density increases, the depth and area of laser ablation increase. Due to the high power density of the laser, the paint film and carbon shell will gasify, and the substrate will melt.

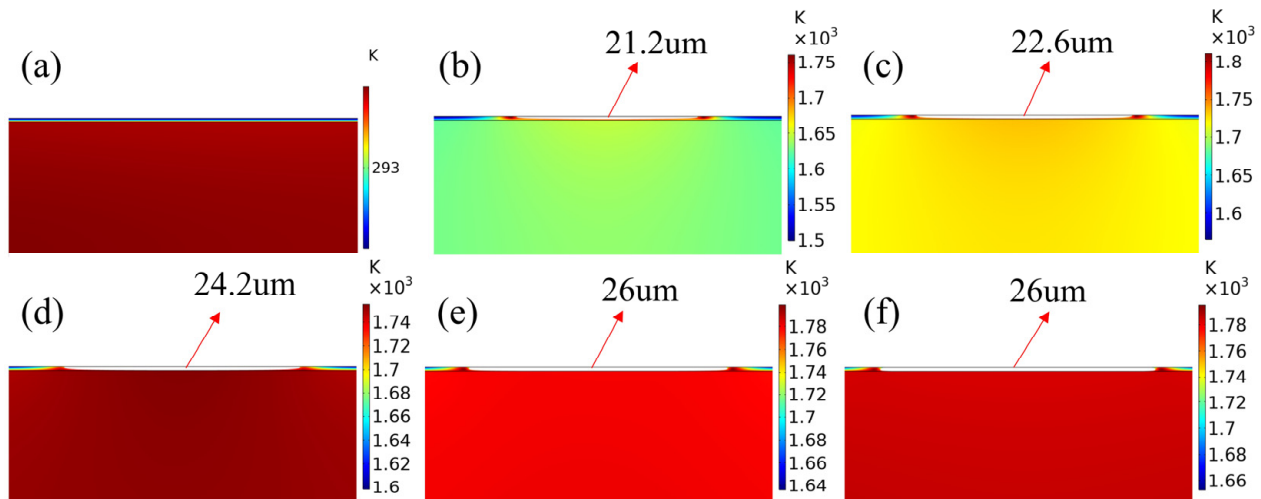


Figure 4. Simulation results of CW laser paint ablation under different power densities: (a) 0 W/cm² (b) 3621 W/cm², (c) 6564 W/cm², (d) 8035 W/cm², (e) 9733 W/cm² (f) 10,865 W/cm².

Figure 5 shows the experimental results of CW laser paint removal. It can be found that as the laser power density increases, the depth and area of laser ablation increase. When the laser power density is 6564 W/cm², the maximum ablation depth of the material is close to the thickness of the paint film, exposing part of the bright metal substrate, as shown in Figure 5c. However, ring-shaped contaminants remain on the material’s surface after laser paint removal.

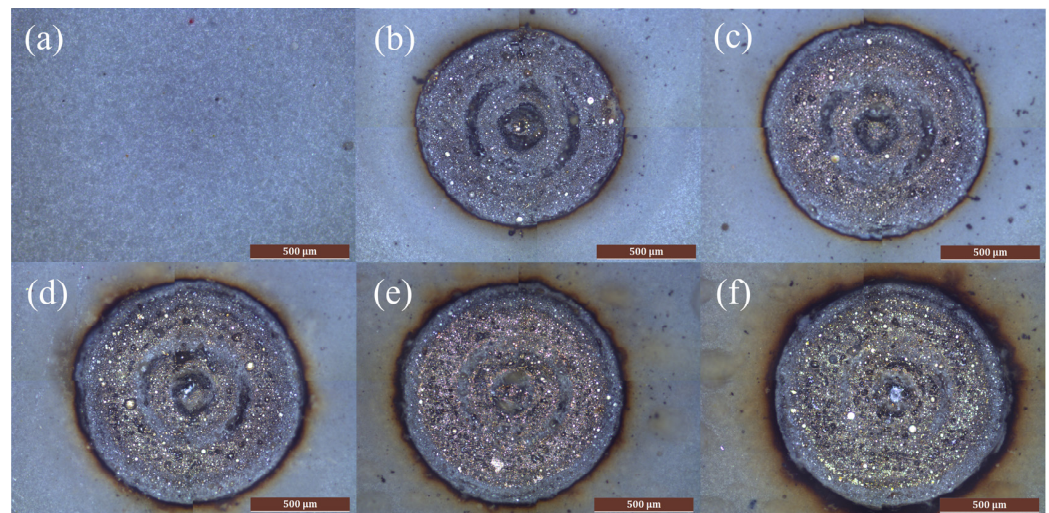


Figure 5. Experimental results of CW laser paint removal under different power densities: (a) 0 W/cm^2 (b) 3621 W/cm^2 , (c) 6564 W/cm^2 , (d) 8035 W/cm^2 , (e) 9733 W/cm^2 (f) 10865 W/cm^2 .

Since the laser is a Gaussian beam, the temperature at the center of the laser is different from the temperature at the boundary during laser paint removal. After the paint film melts, the temperature gradient and the Marangoni effect cause the paint film to flow during the laser paint removal. The paint film flows at different speeds at the spot center and the spot boundary. Therefore, on both sides of the boundary between different areas, the flow between the paint films inhibit each other, and deposition occurs at the boundary. During the paint removal, the paint film will continue to flow toward the regional boundary under the influence of the temperature gradient and Marangoni effect, forming ring-shaped paint film residues at the boundary. As the laser power density increases, when the laser power density is $10,865 \text{ W/cm}^2$, a bright substrate is exposed after laser paint removal, and no contaminants remain on the material surface.

5.2. Surface Temperature

Figure 6 shows the evolution of the material surface temperature with time. It can be found from Figure 6 that after the laser is emitted, the surface temperature of the material quickly rises to a peak value and then begins to decrease. The temperature trends obtained from simulations and experiments are almost identical. However, there are significant differences between the temperature values obtained from simulations and experiments. This is because, during the CW laser paint removal experiment, the thermal emissivity of the paint film changes due to gasification and pyrolysis. The temperature measured via a high-speed infrared thermometer is calculated based on the thermal emissivity of the material. Changes in the material's thermal emissivity due to gasification and pyrolysis will cause it to be unable to measure the surface temperature of the material accurately. Therefore, the material surface temperatures obtained from simulations and experiments are different. Since the temperature trends obtained by simulation and experiment are almost the same, the temperature obtained by simulation results is more accurate than that of experiment.

In addition, the surface temperature of the material drops rapidly after reaching its peak value. During the CW laser paint removal, the gasification and pyrolysis of the paint film surface will leave a carbon shell on the surface. Since the thermal conductivity of the carbon shell is lower than that of the epoxy paint film, the temperature of the material rises faster after the paint film is pyrolyzed. As the laser irradiation time increases, the carbon shell begins to gasify. After the carbon shell is ablated, the exposed aluminum alloy substrate has a high reflectivity to the laser. As a result, the rate at which the material absorbs laser energy decreases, causing the temperature of the material to decrease.

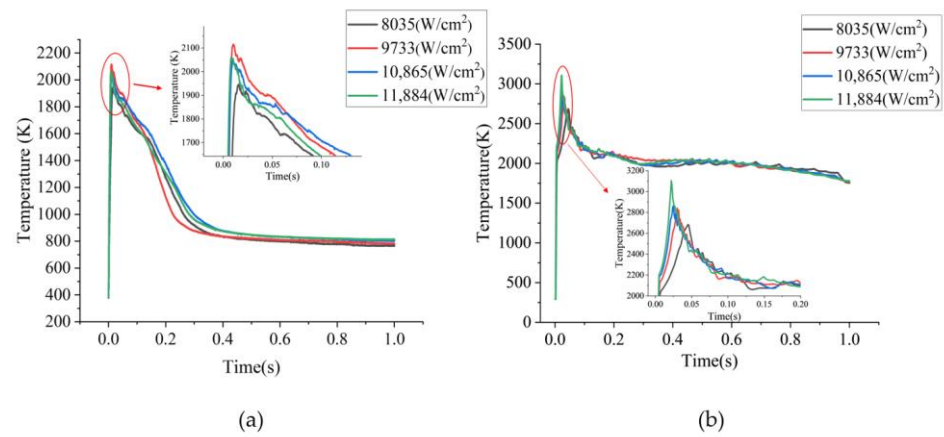


Figure 6. The evolution of material surface temperature with time: (a) experimental result, (b) simulation results.

5.3. Ablation Depth

Figure 7 shows the variation of ablation depth with laser power density. Due to the uncertainty of in-depth measurement, we measured five times and took the average, reducing the impact of depth measurement uncertainty. By comparing simulation and experimental results, it was found that the depth of laser paint removal increases linearly with laser power density. It can be found from Figure 7 that when the CW laser power density is 9733 W/cm², the depth of the paint film removed is equal to the thickness of the paint film, and the paint film is completely removed. The simulation results are consistent with the experimental results. This simulation model can accurately predict the CW laser paint removal threshold.

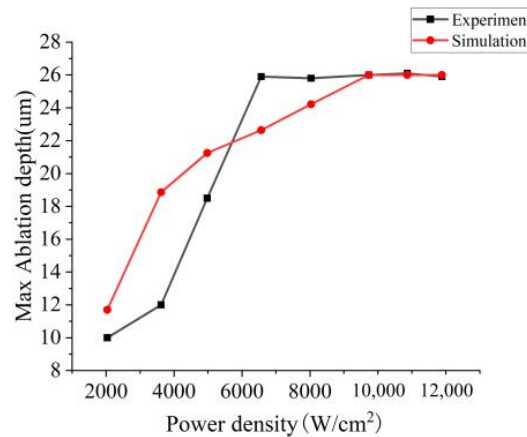


Figure 7. The simulation and experimental results of laser paint removal depth with laser power density.

5.4. 3D Surface Profile

It can be found from Figure 6 that as the laser power density increases, the material surface after laser paint removal becomes smoother and smoother. By measuring the surface roughness of the material, we found that as the laser power density increases, the surface roughness of the material shows a downward trend, as shown in Figure 8. However, when the laser power density is 4979–8035 W/cm², the surface roughness of the material first increases and then decreases as the laser power density increases. The remaining paint film and exposed aluminum alloy substrate after laser paint removal increase the roughness of the material surface.

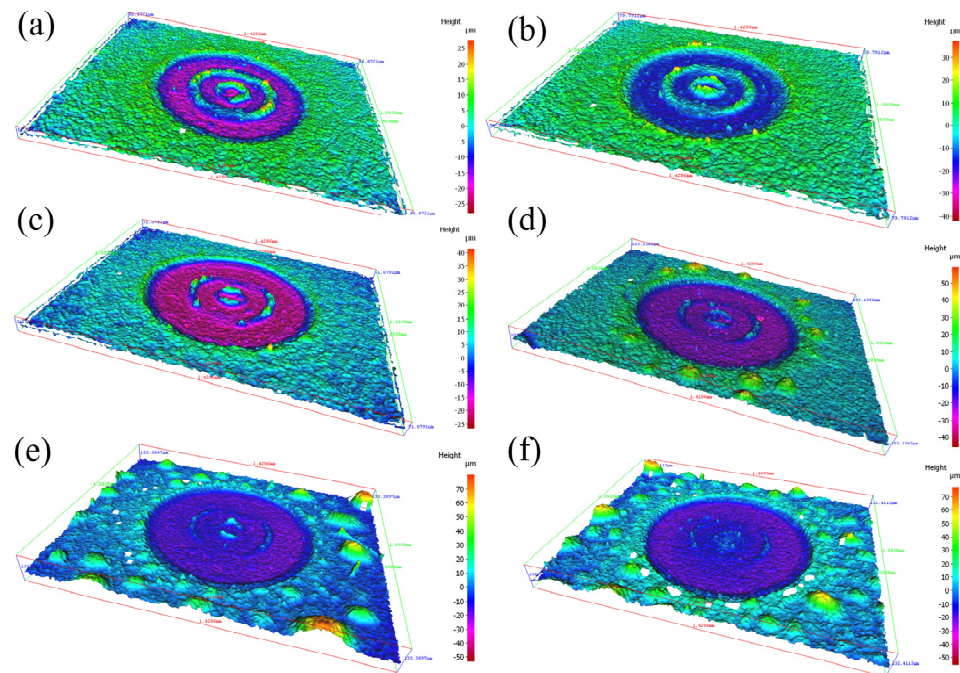


Figure 8. The three-dimensional surface profile of the material after laser paint removal: (a) 3621 W/cm², (b) 4979 W/cm², (c) 6564 W/cm², (d) 8035 W/cm², (e) 9733 W/cm², (f) 10,865 W/cm².

Figure 9 shows the variation of material surface roughness with laser power density. When the CW laser power density is the paint removal threshold, the roughness of the material surface is 1.67 μm, which is significantly smaller than the roughness of the original substrate of the aluminum alloy material (2 μm). The surface roughness of the material is reduced after CW laser removal. It can be found from the simulation that when the laser power density is high, the temperature of the aluminum alloy substrate material exceeds its melting temperature and melts, as shown in Figure 4. Therefore, the decrease in surface roughness of the material after laser paint removal is caused by the melting of the aluminum alloy substrate material.

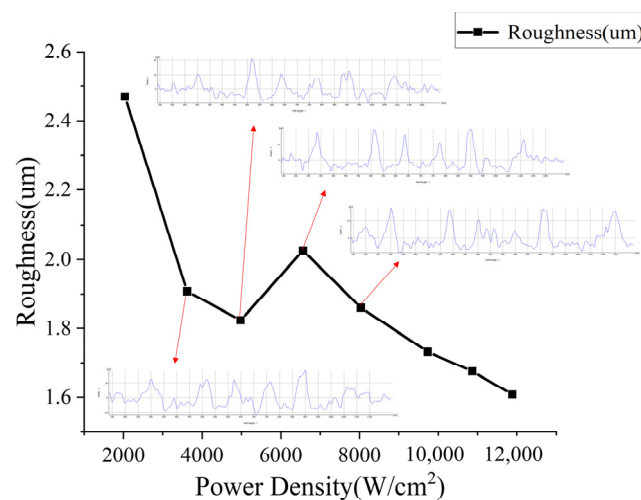


Figure 9. Material surface roughness with laser power density.

6. Conclusions

This paper establishes a CW laser thermal paint removal model based on the heat conduction equation and Arrhenius’ law, considering the paint film and carbon shell’s gasification. The CW laser paint removal was studied through simulations and experiments.

We found that the ablation depth of a CW laser increases with increasing laser power density. The paint film was removed entirely when the CW laser power density was 10,865 W/cm². During CW laser paint removal, due to the pyrolysis of the paint film material and the reflection of the laser by the substrate, the surface temperature of the material increases rapidly, reaches a peak, and then decreases. By comparing the simulation and experimental results, it can be found that the simulation and experimental results are consistent. The established simulation model can accurately predict the CW laser paint removal threshold. In addition, after laser paint removal, the surface roughness of the material is reduced due to the melting of the substrate. Therefore, by designing reasonable CW laser parameters, laser paint removal and polishing can be achieved simultaneously.

Author Contributions: Conceptualization, Y.L. and W.Z.; methodology, G.J.; software, H.D.; validation, J.L., W.Z. and G.J.; formal analysis, Y.L.; investigation, G.J.; resources, W.Z.; data curation, J.L.; writing—original draft preparation, Y.L.; writing—review and editing, Y.L.; visualization, Y.L.; supervision, H.D.; project administration, W.Z.; funding acquisition, G.J. All authors have read and agreed to the published version of the manuscript.

Funding: This research was funded by the National Natural Science Foundation of China, grant number U19A2077, and the Changchun Science and Technology Development Plan, grant number 21ZY34, and the Jilin Provincial Department of Education Science and Technology Research, grant number JJKH20230792KJ.

Institutional Review Board Statement: Not applicable.

Informed Consent Statement: Not applicable.

Data Availability Statement: The data supporting this study's findings are available from the corresponding author upon reasonable request.

Conflicts of Interest: The authors declare that they have no known competing financial interests or personal relationships that could have appeared to influence the work reported in this paper.

References

1. Park, J.E.; Kyung, K.S.; Moon, M.G.; Yun, I.S.; Eum, M.J. Applicability evaluation of clean laser system in surface preparation on steel. *Int. J. Steel Struct.* **2020**, *20*, 1882–1890. [[CrossRef](#)]
2. Barletta, M.; Gisario, A.; Tagliaferri, V. Advance in paint stripping from aluminium substrates. *J. Mater. Process. Technol.* **2006**, *173*, 232–239. [[CrossRef](#)]
3. Schmidt, M.J.J.; Li, L.; Spencer, J.T. An investigation into the feasibility and characteristics of using a 2.5 kW high power diode laser for paint stripping. *J. Mater. Process. Technol.* **2003**, *138*, 109–115. [[CrossRef](#)]
4. Turner, M.W.; Crouse, P.L.; Li, L.; Smith, A.J.E. Investigation into CO₂ laser cleaning of titanium alloys for gas-turbine component manufacture. *Appl. Surf. Sci.* **2006**, *252*, 4798–4802. [[CrossRef](#)]
5. Chen, G.X.; Kwee, T.J.; Tan, K.P.; Choo, Y.S.; Hong, M.H. Laser cleaning of steel for paint removal. *Appl. Phys. A* **2010**, *101*, 249–253. [[CrossRef](#)]
6. Madhukar, Y.K.; Mullick, S.; Shukla, D.K.; Kumar, S.; Nath, A.K. Effect of laser operating mode in paint removal with a fiber laser. *Appl. Surf. Sci.* **2013**, *264*, 892–901. [[CrossRef](#)]
7. Madhukar, Y.K.; Mullick, S.; Nath, A.K. Development of a water-jet assisted laser paint removal process. *Appl. Surf. Sci.* **2013**, *286*, 192–205. [[CrossRef](#)]
8. Guerrero, G.R.; Sevilla, L.; Soriano, C. Laser and pyrolysis removal of fluorinated ethylene propylene thin layers applied on en AW-5251 aluminium substrates. *Appl. Surf. Sci.* **2015**, *353*, 686–692. [[CrossRef](#)]
9. Anthofer, A.; Lippmann, W.; Hurtado, A. Laser decontamination of epoxy painted concrete surfaces in nuclear plants. *Opt. Laser Technol.* **2014**, *57*, 119–128. [[CrossRef](#)]
10. Anthofer, A.; Kögler, P.; Friedrich, C.; Lippmann, W.; Hurtado, A. Laser decontamination and decomposition of PCB-containing paint. *Opt. Laser Technol.* **2017**, *87*, 31–42. [[CrossRef](#)]
11. Lu, Y.; Yang, L.; Wang, Y.; Chen, H.; Guo, B.; Tian, Z. Paint removal on the 5A06 aluminum alloy using a continuous wave fiber laser. *Coatings* **2019**, *9*, 488. [[CrossRef](#)]
12. Penide, J.; Quintero, F.; Riveiro, A.; Sánchez-Castillo, A.; Comesaña, R.; del Val, J.; Lusquiños, F.; Pou, J. Removal of graffiti from quarry stone by high power diode laser. *Opt. Lasers Eng.* **2013**, *51*, 364–370. [[CrossRef](#)]
13. Provines, J.; Rickard, R.; Sharp, S. Evaluation of a Continuous Laser Ablation Coating Removal Device for Steel Bridges. *Transp. Res. Rec.* **2022**, *2676*, 767–778. [[CrossRef](#)]

14. Li, W.; Su, X.; Gu, J.; Jin, Y.; Xu, J.; Guo, B. Removal Mechanisms and Microstructure Characteristics of Laser Paint Stripping on Aircraft Skin Surface. *Photonics* **2023**, *10*, 96. [[CrossRef](#)]
15. Zhao, Z.; Liu, X.; Chen, Z.; Tian, Y.; Chen, M.; Liu, L.; Song, F. Evaluation of laser cleaning effect for the removal of paint on aluminum alloys. *Int. J. Adv. Manuf. Technol.* **2023**, *126*, 3193–3203. [[CrossRef](#)]
16. Liu, Q.; Zhao, Y.; Meng, J.; Wang, K.; Zhao, G.; Li, L.; Zheng, Z.; Liu, G.; Cao, C.; Dai, D. Research on the Removal Mechanism of Resin-Based Coatings by Water Jet-Guided Quasi-Continuous Laser Cleaning. *Appl. Sci.* **2022**, *12*, 5450. [[CrossRef](#)]
17. Bauerle, D. *Laser Processing and Chemistry*, 4th ed.; Springer: Heidelberg, Germany, 2011; p. 21.
18. Ben-Yakar, A.; Byer, R.L. Femtosecond laser ablation properties of borosilicate glass. *J. Appl. Phys.* **2004**, *96*, 5316–5323. [[CrossRef](#)]
19. Chen, Y.Z.; Xie, X.D.; Xiao, X.P. An evolving model of surface profile produced by nanosecond laser ablation on aluminum alloy. *J. Laser Micro Nanoeng.* **2019**, *14*, 152–160.
20. Qin, R.; Yang, H. Numerical Simulation of Temperature Field for Laser Removal of Oxide Layer of AlSi10Mg (Fe) Aluminum Alloy. *Integr. Ferroelectr.* **2022**, *229*, 158–172. [[CrossRef](#)]
21. Esfahani, J.A.; Sousa, A.C. Ignition of epoxy by a high radiation source. A numerical study. *Int. J. Therm. Sci.* **1999**, *38*, 315–323. [[CrossRef](#)]
22. Ohkubo, T.; Sato, Y.; Matsunaga, E.I.; Tsukamoto, M. Thermal effect of laser ablation on the surface of carbon fiber reinforced plastic during laser processing. *Appl. Phys. A* **2018**, *124*, 149. [[CrossRef](#)]
23. Zou, W.F.; Xie, Y.M.; Xiao, X.; Zeng, X.; Zeng, X.Z.; Luo, Y. Application of thermal stress model to paint removal by Q-switched Nd: YAG laser. *Chin. Phys. B* **2014**, *23*, 433–438. [[CrossRef](#)]
24. Papadopoulos, K.; Tserpes, K. Analytical and Numerical Modeling of Stress Field and Fracture in Aluminum/Epoxy Interface Subjected to Laser Shock Wave: Application to Paint Stripping. *Materials* **2022**, *15*, 3423. [[CrossRef](#)] [[PubMed](#)]
25. Lu, X.D. Study on Ignition and Combustion Characteristics of Polymer. Master's Thesis, Qingdao University of Science and Technology, Qingdao, China, 2007.
26. Richter, A.; Nikrityuk, P.A.; Meyer, B. Three-dimensional calculation of a chemically reacting porous particle moving in a hot O₂/CO₂ atmosphere. *Int. J. Heat Mass Transf.* **2015**, *83*, 244–258. [[CrossRef](#)]
27. Lascano, D.; Lerma-Canto, A.; Fombuena, V.; Balart, R.; Montanes, N.; Quiles-Carrillo, L. Kinetic analysis of the curing process of biobased epoxy resin from epoxidized linseed oil by dynamic differential scanning calorimetry. *Polymers* **2021**, *13*, 1279. [[CrossRef](#)]
28. Stauch, R.; Maas, U. Transient detailed numerical simulation of the combustion of carbon particles. *Int. J. Heat Mass Transf.* **2009**, *52*, 4584–4591. [[CrossRef](#)]
29. Roberts, D.E. Pulsed laser coating removal by detachment and ejection. *Appl. Phys. A-Mater. Sci. Process* **2004**, *79*, 1067–1070. [[CrossRef](#)]

Disclaimer/Publisher's Note: The statements, opinions and data contained in all publications are solely those of the individual author(s) and contributor(s) and not of MDPI and/or the editor(s). MDPI and/or the editor(s) disclaim responsibility for any injury to people or property resulting from any ideas, methods, instructions or products referred to in the content.